Proceedings of the ASME 2016 Dynamic Systems and Control Conference
DSCC 2016
October 12–14, 2016, Minneapolis, Minnesota, USA

DSCC2016-9912

VARIATIONS ON THE ROLE OF PRINCIPAL CONNECTIONS IN ROBOTIC LOCOMOTION

Tony Dear*
Robotics Institute
Carnegie Mellon University
Pittsburgh, Pennsylvania 15213
tonydear@cmu.edu

Scott David Kelly
Department of Mechanical Engineering
and Engineering Science
University of North Carolina at Charlotte
Charlotte, North Carolina 28223
scott@kellyfish.net

Howie Choset
Robotics Institute
Carnegie Mellon University
Pittsburgh, Pennsylvania 15213
choset@cs.cmu.edu

ABSTRACT

Diverse problems in robotic locomotion have previously been modeled in terms of connections on principal bundles. Ordinarily, one identifies points in the base manifold of such a bundle with different internal configurations of a robot, identifies points in the fiber over a given base point with different positions and orientations of the robot in its environment, and assumes control to be applied in the former but not the latter. We examine ways in which the ordinary application of this theory may be adapted to problems in aquatic and terrestrial locomotion that fail to accommodate the preceding description.

1 INTRODUCTION

A modeling paradigm centered on the geometric notion of a *principal fiber bundle* has emerged in recent decades to accommodate a variety of problems in robotic locomotion, facilitating tasks like the assessment of controllability and algorithmic motion planning. The standard implementation of this paradigm is illustrated by the following example.

Example 1.1 (*Elliptical swimmer with a movable internal mass*)**.** Fig. 1 depicts a hollow elliptical cylinder surrounded by an inviscid planar fluid with no outer boundary. The fluid is assumed to be at rest infinitely far away. Interior to the cylinder is a point mass. The cylinder has no mass of its own, but since fluid is moved when the cylinder is moved, the cylinder exhibits both a nonzero effective mass that depends on its direction of translation and a nonzero effective rotational inertia. Actuation couples the cylinder to the point mass. A force between the two that induces the position of the point mass relative to the cylinder to vary cyclically may result in acyclic movement of the cylinder through its environment as a result of the cylinder's anisotropic effective mass, even if the system is initially at rest and the net momentum remains zero thereafter.

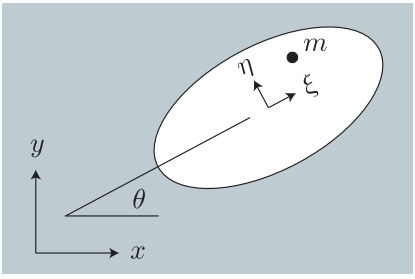

FIGURE 1. A HOLLOW ELLIPTICAL SWIMMER IN A PLANAR IDEAL FLUID. THE EFFECTIVE MASS OF THE ELLIPTICAL CYLINDER DEPENDS ON ITS DIRECTION OF MOTION, SO CYCLIC DISPLACEMENTS OF THE INTERNAL MASS RELATIVE TO THE CYLINDER CAN RESULT IN NET LOCOMOTION.

The manifold of configurations available to this system is naturally the Cartesian product of the manifold comprising all possible positions and orientations of the ellipse relative to a stationary frame of reference and the manifold comprising all pos-

*Address all correspondence to this author.

sible positions of the point mass relative to a frame of reference attached to the ellipse. The former is the Lie group SE(2) and the latter $\mathbb{R}^2$. Endowed with the operation of vector addition, the latter is as much a Lie group as the former, but the former and not the latter constitutes a *symmetry group* for the system. This statement will be made mathematically precise below, but intuitively it means that the system's dynamics are independent of the position and orientation of the ellipse. The system's dynamics are *not* independent of the position of the point mass relative to the ellipse because the effective rotational inertia of the ellipse and mass together vary when this position varies.

If M_{long}, M_{lat}, and M_{rot} denote the longitudinal effective mass and lateral effective mass of the ellipse and the effective rotational inertia of the ellipse relative to its center, respectively, and if (x,y) and (ξ,η) denote the position of the center of the ellipse relative to a stationary frame of reference and the position of the internal mass relative to a frame of reference affixed to the center of the ellipse, respectively (as shown in Fig. 1), then the total kinetic energy in the system is given by

$$L = \frac{1}{2}M_{\text{long}}v_{\text{long}}^2 + \frac{1}{2}M_{\text{lat}}v_{\text{lat}}^2 + \frac{1}{2}M_{\text{rot}}\dot{\theta}^2 + \frac{1}{2}mv_{\text{point mass}}^2,$$

where

$$v_{\text{long}} = \dot{x}\cos\theta + \dot{y}\sin\theta, \qquad v_{\text{lat}} = -\dot{x}\sin\theta + \dot{y}\cos\theta,$$

and $v_{\text{point mass}}$ is the magnitude of

$$\frac{d}{dt}(x + \xi\cos\theta - \eta\sin\theta, y + \xi\sin\theta + \eta\cos\theta).$$

The configuration manifold $Q = \text{SE}(2)\times\mathbb{R}^2$ may be thought of as a bundle over $\mathbb{R}^2$. Left translation in SE(2) defines a fiber-preserving action

$$\Phi : \text{SE}(2)\times Q \to Q : (g,q) \mapsto \Phi_g q$$

that's free and transitive on each fiber. This action endows Q with the structure of a *principal* bundle with *base space* $B = \mathbb{R}^2$ and *structure group* $G = \text{SE}(2)$ — that is, a bundle over B with fibers that are homeomorphic to G but lack the inhomogeneity that is present in G due to the existence of a preferred identity element.

The Lagrangian L is invariant under the tangent-lifted action of SE(2) on TQ corresponding to the action Φ. This is the sense in which SE(2) is a symmetry group for the system. Because of this invariance, L determines a *principal connection* on the bundle Q — that is, a splitting of the tangent space T_qQ at each point $q \in Q$ into subspaces H_qQ and V_qQ such that

$$H_{\Phi_g q}Q = (T_q\Phi(g,\cdot))(H_qQ)$$

for $g \in G$. At each $q \in Q$, H_qQ is isomorphic to $T_{\pi(q)}B$, where $\pi : Q \to B$ denotes the canonical projection.

A principal connection determines a unique lifting of tangent vectors in T_bB to tangent vectors in H_qQ at each $q \in \pi^{-1}b$. The invariance of L under left translation in SE(2) implies, via *Noether's theorem* [1], that the dynamics of the system in Fig. 1 conserve linear and angular momentum. The physical interpretation of the connection is that whenever the internal mass is actuated to move relative to the ellipse, the velocity of the mass relative to the ellipse uniquely determines the velocity of the ellipse relative to the stationary frame because of this conservation law, and that the latter depends on the position and orientation of the ellipse only via rotation by the angle θ.

Specifically, if the total linear and angular momentum in the system are zero initially, then the velocity of the ellipse satifies

$$\begin{bmatrix}\dot{x}\\ \dot{y}\\ \dot{\theta}\end{bmatrix} = -\begin{bmatrix}\cos\theta & -\sin\theta & 0\\ \sin\theta & \cos\theta & 0\\ 0 & 0 & 1\end{bmatrix} A(\xi,\eta)\begin{bmatrix}\dot{\xi}\\ \dot{\eta}\end{bmatrix},$$

where

$$A(\xi,\eta) = \frac{m}{\Delta}\begin{bmatrix}(m+M_{\text{lat}})M_{\text{rot}} + mM_{\text{lat}}\xi^2 & mM_{\text{lat}}\xi\eta\\ mM_{\text{long}}\xi\eta & (m+M_{\text{long}})M_{\text{rot}} + mM_{\text{long}}\eta^2\\ -(m+M_{\text{lat}})M_{\text{long}}\eta & (m+M_{\text{long}})M_{\text{lat}}\xi\end{bmatrix}$$

with

$$\Delta = m(m+M_{\text{lat}})M_{\text{long}}\eta^2 + (m+M_{\text{long}})((m+M_{\text{lat}})M_{\text{rot}} + mM_{\text{lat}}\xi^2).$$

The differential form on B represented by the matrix $A(\xi,\eta)$ is called the *local connection form*.

It is shown in [2] that for an ellipse with semi-major axis a and semi-minor axis b in a fluid with density ρ,

$$M_{\text{long}} = \pi\rho b^2, \quad M_{\text{lat}} = \pi\rho a^2, \quad M_{\text{rot}} = \frac{1}{8}\pi\rho\left(a^2+b^2\right)^2.$$

Fig. 2 depicts the acyclic motion from rest of an ellipse with $a = 2$ and $b = 1/2$ in a fluid with density $\rho = 1/4$ corresponding to the cyclic motion of an internal mass with $m = 1$ relative to the center of the ellipse. Because the system is modeled by a principal connection, the path traced in B (with coordinates ξ and η) determines the path traced in G (with coordinates x, y, and θ) in a manner independent of time parametrization. Since only the

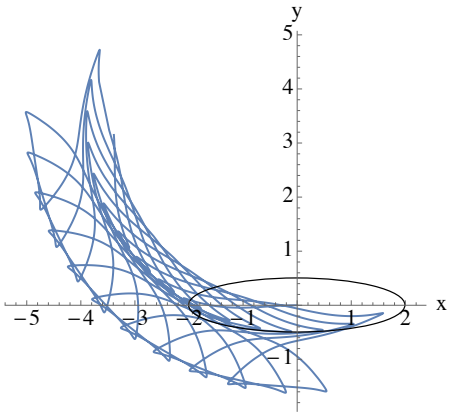

FIGURE 2. TRAJECTORY OF AN ELLIPTICAL CYLINDER RESULTING FROM ACTUATION OF AN INTERNAL MASS SUCH THAT $(\xi,\eta) = (1-\cos 3t, 2\sin 2t)$. THE SYSTEM IS INITIALLY AT REST AT THE ORIGIN; THE TOTAL LINEAR AND ANGULAR MOMENTUM IN THE SYSTEM REMAIN ZERO FOR ALL TIME.

geometry of the path in B matters, the net relative displacement in G associated with a closed path in B — or more properly, the element $h \in G$, which is independent of the starting point in G, such that Φ_h corresponds to the net relative displacement resulting from a single closed loop along this path — is called the *geometric phase* associated with this closed path.

□

Certain features of Ex. 1.1 — specifically, the identification of the system's position and orientation with the symmetry group defining the fiber and the assumption that actuation takes place on the base space — are ubiquitous in the literature framing robotic locomotion in terms of connections on principal bundles. Early contributions to this literature include treatments of bodies reorienting themselves in space using momentum wheels [3, 4], deformable swimmers in Stokes flows [5, 6] and in ideal flows [7], and wheeled mobile robots subject to no-slip rolling constraints [8, 9]. In the present paper, we show that these features are not universal by analyzing two locomotion problems in which the underlying dynamics evolve on principal bundles, but the symmetry group corresponds to the space of internal shapes and/or actuation is applied other than on the base space.

The system in Sec. 2 resembles the system in Ex. 1.1 in that it comprises a rigid cylinder with time-varying nonuniform density in an ideal fluid, but the asymmetry that enables locomotion is one in the surrounding environment rather than in the shape of the cylinder. As a result, the space of internal shapes on which actuation occurs constitutes the symmetry group for the system. A novel consequence of this is a recasting of the *scallop theorem* that is normally invoked to assert — by extrapolation from its initial presentation in the context of a hinged swimmer in a Stokes flow [10] — that a system with mechanics modeled by a principal connection must vary at least two internal degrees of freedom over time to achieve nonzero net locomotion through cyclic shape changes. The theorem correctly reflects the idea that the geometric phase associated with a closed path in the base space of a principal bundle with an associated connection will be nonzero only if the path encloses nonzero area, requiring variations in at least two base directions. In the context of Sec. 2, net locomotion *is* possible through cyclic variation in only one internal degree of freedom because the system's internal degrees of freedom correspond to fiber variables rather than base variables. For this system, the scallop theorem asserts that if actuation were applied upon the cylinder from without rather than within, then a cyclic motion of the cylinder through its environment would have to involve translation in two directions if it were to generate a net change in the cylinder's internal mass distribution.

The system in Sec. 3, a terrestrial robot comprising three wheeled links joined at hinges resting atop a horizontal platform, is more conventional in the sense that changes in the position and orientation of the robot relative to the platform constitute a symmetry group — again $\mathrm{SE}(2)$, as in Ex. 1.1 — for the system's dynamics. If the robot's wheels roll on the platform without slipping, then kinematic considerations are sufficient to define a connection in the principal bundle with structure group $\mathrm{SE}(2)$ over the base space $\mathbb{T}^2$ comprising all possible hinge angles. This connection was derived in [11], but it was assumed therein that the robot's hinges were subject to direct actuation. In the present paper, we replace actuation at the robot's hinges with torsional springs and examine the locomotion that results when the platform supporting the robot is induced to vibrate. The principal connection from [11] still determines the relationship between variations in the shape of the robot and its motion relative to the platform, but energy is introduced to the system in a manner that favors neither. In fact, when we expand the system's configuration manifold to accommodate planar translation of the platform, we endow this manifold with the structure of a nested principal bundle, fibering the original configuration manifold with copies of $(\mathbb{R}^2,+)$. If the platform has finite mass and the robot-platform system is allowed to evolve freely, then a second principal connection reflecting the overall conservation of linear momentum — a *mechanical connection* as in Ex. 1.1 and Sec. 2 — will dictate the motion of the robot and platform relative to a stationary frame of reference. We introduce actuation on the outer fiber and violate this conservation law, but now study how the system's dynamics naturally select trajectories in the inner bundle that are compatible with the kinematic connection.

2 CIRCULAR SWIMMER NEAR A CORNER

Fig. 3 depicts a hollow circular cylinder surrounded by an inviscid planar fluid that's bounded on two sides by solid walls.

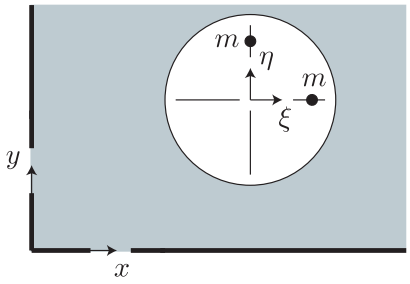

FIGURE 3. A HOLLOW CIRCULAR SWIMMER IN A PLANAR IDEAL FLUID BOUNDED BY TWO SOLID WALLS. THE EFFECTIVE MASS OF THE CYLINDER DEPENDS ON ITS DIRECTION OF MOTION IN A MANNER THAT INCREASES WITH PROXIMITY TO THE WALLS, SO CYCLIC DISPLACEMENTS OF THE INTERNAL MASSES RELATIVE TO THE CYLINDER CAN RESULT IN NET LOCOMOTION.

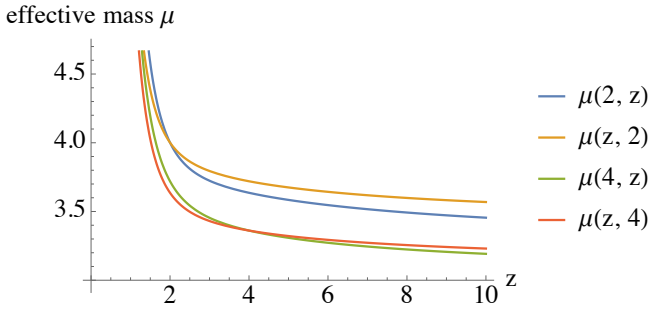

FIGURE 4. EFFECTIVE MASS OF A HOLLOW CIRCULAR CYLINDER WITH UNIT RADIUS IN AN IDEAL FLUID WITH UNIT DENSITY BOUNDED ON TWO SIDES BY PERPENDICULAR SOLID WALLS. THE QUANTITY $\mu(x,y)$ REPRESENTS THE EFFECTIVE MASS ASSOCIATED WITH MOTION IN THE x DIRECTION WHEN THE CYLINDER IS A DISTANCE x FROM ONE WALL AND A DISTANCE y FROM THE OTHER. INFINITELY FAR FROM BOTH WALLS, THE CYLINDER'S EFFECTIVE MASS EQUALS π.

The fluid is assumed to be at rest infinitely far away. Interior to the cylinder are two point masses that are actuated to translate relative to the cylinder along axes passing through the cylinder's center, parallel to the walls bounding the fluid. These axes are defined relative to the cylinder, but no mechanism is present whereby the cylinder can be induced to rotate. Actuation that induces either mass to translate relative to the cylinder will induce the cylinder to translate in the opposite direction. In the absence of the walls, the conservation of linear momentum would imply that any periodic displacement of one or both masses relative to the cylinder must result in a periodic movement of the cylinder through its environment. In the presence of the walls, periodic displacement of one or both masses relative to the cylinder will result in *acyclic* motion of the cylinder because the cylinder's effective mass depends on its proximity to the walls.

If the cylinder's distances from each wall are not equal, then its effective mass will differ for different directions of motion. A closed-form expression for the cylinder's effective mass as a function of its position and direction of motion is not straightforward to obtain, but a numerical approximation is. If we equate the horizontal and vertical walls with the x and y axes as shown in Fig. 3, then the kinetic energy associated with arbitrary motion of the cylinder can be approximated by a function of the form

$$\mathrm{KE} = \frac{1}{2}M_x(x,y)\dot{x}^2 + \frac{1}{2}M_y(x,y)\dot{y}^2 = \frac{1}{2}\mu(x,y)\dot{x}^2 + \frac{1}{2}\mu(y,x)\dot{y}^2,$$

where the asymmetry of the function $\mu(\cdot,\cdot)$ relative to its two arguments reflects the asymmetric effect of each wall on tangential versus normal movement of the cylinder. Fig. 4 depicts this asymmetry in terms of some representative choices of the two arguments. The approximation to $\mu(\cdot,\cdot)$ represented in Fig. 4 was obtained by solving Laplace's equation numerically, computing the corresponding kinetic energy in the system with the cylinder translating horizontally with unit speed from each point in a uniform spatial grid, and by fitting a smooth function to the resulting table of results.

If the masses are actuated to move relative to the cylinder so that the horizontal relative displacement ξ of the one and the vertical relative displacement η of the other vary with time, then the resulting dynamics in the cylinder's displacement will satisfy Lagrange's equations relative to the Lagrangian

$$L = \frac{1}{2}\mu(x,y)\dot{x}^2 + \frac{1}{2}\mu(y,x)\dot{y}^2 + \frac{1}{2}m(\dot{x}+\dot{\xi})^2 + \frac{1}{2}m(\dot{y}+\dot{\eta})^2.$$

This Lagrangian is invariant under the tangent lift of the action of the Lie group $(\mathbb{R}^2,+)$ on $Q=\mathbb{R}^4$ given by

$$\Phi : \mathbb{R}^2 \times Q \to Q : ((a,b),(x,y,\xi,\eta)) \mapsto (x,y,\xi+a,\eta+b).$$

This is *not* true of the action

$$\Phi : \mathbb{R}^2 \times Q \to Q : ((a,b),(x,y,\xi,\eta)) \mapsto (x+a,y+b,\xi,\eta),$$

and the x and y components of the effective linear momentum satisfy the evolution equations

$$\begin{aligned} \frac{d}{dt}\Big(M_x\dot{x} + m(\dot{x}+\dot{\xi})\Big) &= \frac{1}{2}\frac{\partial M_x}{\partial x}\dot{x}^2 + \frac{1}{2}\frac{\partial M_y}{\partial x}\dot{y}^2 \\ \frac{d}{dt}\Big(M_y\dot{y} + m(\dot{y}+\dot{\eta})\Big) &= \frac{1}{2}\frac{\partial M_x}{\partial y}\dot{x}^2 + \frac{1}{2}\frac{\partial M_y}{\partial y}\dot{y}^2. \end{aligned} \tag{1}$$

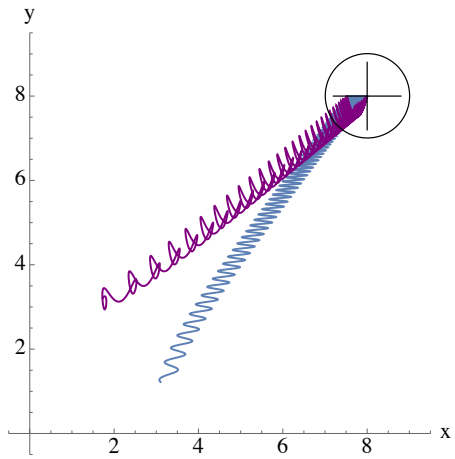

FIGURE 5. TRAJECTORIES OF A CIRCULAR CYLINDER WITH UNIT RADIUS, INITIALLY AT REST IN THE LOCATION SHOWN, RESULTING FROM ACTUATION OF TWO INTERNAL MASSES SUCH THAT $(\xi,\eta) = (1-\cos t, 0)$ (BLUE) and $(\xi,\eta) = (1-\cos t, 1-\cos 2t)$ (PURPLE) WITH $m = \rho = 1$.

It follows that the accelerations of the cylinder and the two masses satisfy

$$(M_x+m)\ddot{x}+m\ddot{\xi} = \frac{1}{2}\frac{\partial M_y}{\partial x}\dot{y}^2 - \frac{1}{2}\frac{\partial M_x}{\partial x}\dot{x}^2 - \frac{\partial M_x}{\partial y}\dot{x}\dot{y}$$
$$(M_y+m)\ddot{y}+m\ddot{\eta} = \frac{1}{2}\frac{\partial M_x}{\partial y}\dot{x}^2 - \frac{1}{2}\frac{\partial M_y}{\partial y}\dot{y}^2 - \frac{\partial M_y}{\partial x}\dot{x}\dot{y}.$$

Fig. 5 depicts acyclic motion of the cylinder from rest corresponding to two different cyclic motions of the internal masses. In one case, $\eta = 0$ for all time to emphasize that net displacement of the cylinder will result even if no area is enclosed by the path in the (ξ,η) plane corresponding to the motion of the masses. Since $\mu(\cdot,\cdot)$ is monotonically decreasing in both of its arguments, the right-hand sides of both equations in (1) are necessarily nonpositive. The cylinder is attracted to the corner in Fig. 5 accordingly. It remains the case, however, that the motion of the cylinder depends on the motion of the internal masses in a manner independent of time parameterization.

3 SNAKE ON A PLANE

In this section, we turn our attention to the three-link terrestrial snake robot shown in Fig. 6. As described previously, this system moves on a horizontal platform and thus has a symmetry group of SE(2). The kinematic connection that relates trajectories in its hinge angles to trajectories in the fiber can be derived using the three independent nonholonomic constraints that prevent the wheels on each of the links from slipping laterally.

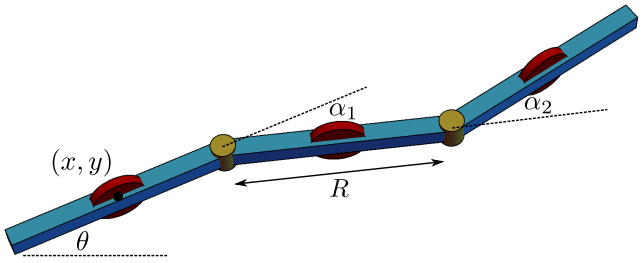

FIGURE 6. A WHEELED ROBOT WITH THREE EQUAL-LENGTH LINKS. (x,y,θ) SPECIFY THE INERTIAL POSITION AND ORIENTATION OF THE FIRST LINK, AND (α_1,α_2) SPECIFY THE RELATIVE ANGLES OF THE LINKS THEREAFTER.

Since the number of constraints is equal to the dimension of the fiber, researchers have also referred to this system as the three-link *kinematic* snake [12–14].

System Model

In this paper, we will assume that the robot's three links are all of equal length R. The robot's configuration manifold is $Q = \mathrm{SE}(2)\times B$, where the fiber variables $g = (x,y,\theta)^T$ specify the position and orientation of the first link and the base space $B = \mathbb{T}^2$ consists of all joint angle configurations $\alpha = (\alpha_1,\alpha_2)^T$ of the robot. In the literature, past work has traditionally assumed that these joint variables are directly controllable, although we will deviate from this setup later in this paper.

The wheels at the centers of the links provide a set of nonholonomic constraints that restrict the system's motion. Each of the constraints can be written in the form

$$-\dot{x}_i\sin\theta_i + \dot{y}_i\cos\theta_i = 0, \tag{2}$$

where $(\dot{x}_i,\dot{y}_i)$ is the velocity and θ_i is the orientation of the ith link. These quantities can be found via the system's geometry and written in terms of the configuration coordinates and velocities. The group and shape velocity components can be separated in Pfaffian form [14] as

$$\omega_g(q)\dot{g} + \omega_\alpha(\alpha)\dot{\alpha} = 0, \tag{3}$$

where $\omega_g \in \mathbb{R}^{3\times 3}$ and $\omega_\alpha \in \mathbb{R}^{3\times 2}$.

Since the number of independent constraints is equal to the dimension of the group, these equations are sufficient to derive a kinematic connection for the system [14]. In other words, the constraint equations fully describe the first-order dynamics of the group variables in terms of the shape variables only, in a form analogous to that Ex. 1.1. In this case, the equations take the

form

$$\begin{bmatrix} \dot{x} \\ \dot{y} \\ \dot{\theta} \end{bmatrix} = - \begin{bmatrix} \cos\theta & -\sin\theta & 0 \\ \sin\theta & \cos\theta & 0 \\ 0 & 0 & 1 \end{bmatrix} A_k(\alpha)\dot{\alpha}, \tag{4}$$

where

$$A_k(\alpha) = \frac{1}{D} \begin{bmatrix} \frac{R}{2}(\cos\alpha_1 + \cos(\alpha_1 - \alpha_2)) & \frac{R}{2}(1+\cos\alpha_1) \\ 0 & 0 \\ \sin\alpha_1 + \sin(\alpha_1 - \alpha_2) & \sin\alpha_1 \end{bmatrix}$$

with $D = \sin\alpha_1 + \sin(\alpha_1 - \alpha_2) - \sin\alpha_2$. As before, the differential form represented by the matrix $A_k(\alpha)$ is the local kinematic connection form.

In the literature, the kinematic model (4) has yielded rich insights into the three-link robot's locomotion. According to Hatton and Choset [15], Eq. (4) can be integrated over a gait γ to obtain the *body-velocity integral*, a measure of displacement corresponding to the directions along a body-attached frame, rotated from the inertial frame by an angle θ. In the world frame, this measure provides the exact rotational displacement and approximates the translational component, the latter being more precise for gaits of small magnitude.

By viewing each row of $A_k(\alpha)$ as a *connection vector field* and the gait γ as a closed trajectory on each of these fields, one can perform integration and obtain a displacement measure for γ by applying a change of variables along with Stokes' theorem in order to obtain

$$\int A_k(\alpha(t))\dot{\alpha}(t)\,\mathrm{d}t = \int_\gamma A_k(\alpha)\,\mathrm{d}\alpha = \iint_\Gamma \operatorname{curl} A_k(\alpha)\,\mathrm{d}\alpha.$$

Here, we call the integrand of the rightmost expression a *height function* [14, 15], while Γ is the signed area of the portion of curl $\mathbf{A}(r)$ enclosed by γ.

The height functions allow us to easily visualize the effects of a gait over a cycle. Fig. 7 shows the x and θ height functions plotted as 2D surfaces, with the domain being various joint angle configurations and the surface height corresponding to the magnitude of curl $A_k(\alpha)$ (the y component is null everywhere).[1] The x height function is positive everywhere, meaning that any closed loop in joint space will lead to net displacement along the robot's longitudinal direction, although the greatest volume occurs alongside the $\alpha_1 = \alpha_2$ singularity line. On the other hand, the θ function is symmetric about this line and anti-symmetric about $\alpha_1 = -\alpha_2$.

[1] We follow [15] in plotting a scaled arctangent of the height function magnitudes in order to finitely show the singular portions. For the value x, we plot $\frac{1}{k}\arctan(kx)$ instead, where k is positive.

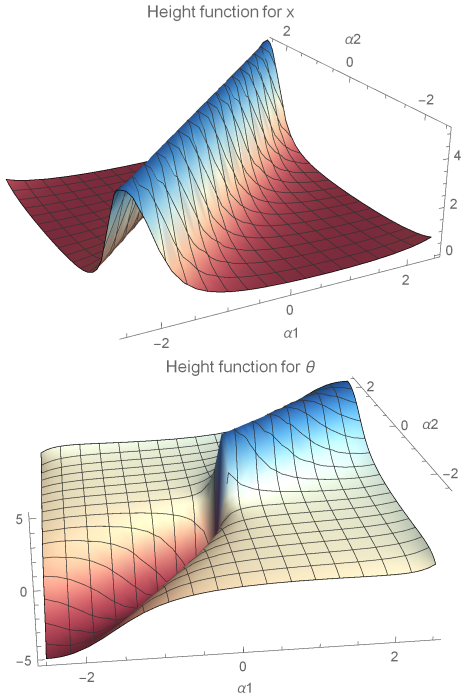

FIGURE 7. THE x AND θ HEIGHT FUNCTIONS CORRESPONDING TO THE LOCAL KINEMATIC CONNECTION. GAITS CAN BE REPRESENTED AS CLOSED CURVES ON THE SURFACES, WHILE THE ENCLOSED VOLUME (SIGNED AREA) APPROXIMATES DISPLACEMENT IN EACH DIRECTION.

Movable Platforms

We now consider a modification to this problem wherein the platform on which the robot moves is itself allowed to move, whether by actuation or in response to the robot's locomotion. The position of the platform, which we denote by (x_p, y_p), is itself a symmetry goup since the modified system's properties do not depend on where the platform is located in space. The configuration manifold is now rewritten as $Q_p = \mathbb{R}^2 \times \mathrm{SE}(2) \times \mathbb{T}^2$, although it is important to note that the connection relationship of Eq. (4) still holds, as the nonholonomic constraints (2) depend solely on how the robot moves relative to the platform.

A Passive Platform In order to determine how the platform's passive movement is related to that of the robot, we can use the fact that a momentum quantity will be conserved using the Lagrangian formulation. Suppose that each of the links has a mass $m_{l,i}$ and an inertia J_i, while the platform has a mass m_p. Denoting the absolute positions of each of the links as $(\tilde{x}_i, \tilde{y}_i) = (x_i, y_i) + (x_p, y_p)$, the Lagrangian of the system is

$$L(q_p, \dot{q}_p) = \frac{1}{2}\sum_{i=1}^{3}\left(m_{l,i}(\dot{\tilde{x}}_i^2 + \dot{\tilde{y}}_i^2) + J_i\dot{\theta}_i^2\right) + \frac{1}{2}m_p(\dot{x}_p^2 + \dot{y}_p^2).$$

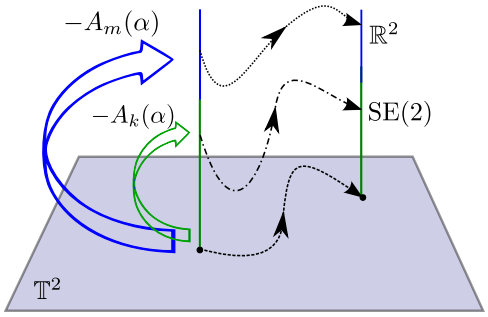

FIGURE 8. THE BUNDLE STRUCTURE OF THE ROBOT AND PASSIVE PLATFORM SYSTEM. TRAJECTORIES IN THE BASE MANIFOLD ARE LIFTED SEPARATELY TO THE ROBOT AND PLATFORM FIBERS VIA THE KINEMATIC AND MECHANICAL CONNECTIONS.

The momentum components are given by the projection of $\frac{\partial L}{\partial \dot{g}}$ onto the directions of motion allowed by the constraints [9]. Since the constraints are independent of $\dot{x}_p$ and $\dot{y}_p$ while completely determining the trajectories of $(\dot{x}, \dot{y}, \dot{\theta})$, the allowable directions of motion are simply the degrees of freedom of the platform. The conserved momenta are given by

$$p = \begin{bmatrix} p_1 \\ p_2 \end{bmatrix} = \begin{bmatrix} \frac{\partial L}{\partial \dot{x}_p} \\ \frac{\partial L}{\partial \dot{y}_p} \end{bmatrix} = \rho_g(q_p)\dot{g} + \rho_\alpha(\alpha)\dot{\alpha}. \tag{5}$$

Noting that the form of Eq. (5) is the same as that of Eq. (3), we can stack them together to obtain a set of full-rank equations, which we can then rearrange to obtain

$$\begin{bmatrix} \dot{x}_p \\ \dot{y}_p \end{bmatrix} = -\begin{bmatrix} \cos\theta & -\sin\theta \\ \sin\theta & \cos\theta \end{bmatrix} A_m(\alpha)\dot{\alpha} + \frac{1}{3m+m_p}\begin{bmatrix} p_1 \\ p_2 \end{bmatrix}. \tag{6}$$

Here, the matrix A_m is the local form of the *mechanical connection*, so named because it is derived from the conservation of momentum for the combined robot-platform system. Bringing Eq. (4) back into the picture, we have two decoupled connections, each dictating how base trajectories evolve separately on each of the two fiber spaces. A graphical representation of how these spaces may be visualized is shown in Fig. 8.

Unlike the form of Eq. (4), there is a drift term in Eq. (6) that depends on the momenta p of the platform. Since the platform is not actuated, Lagrange's equations simply state that $\dot{p} = 0$. Furthermore, if the platform starts from rest so that $p = 0$, the drift terms drop out and the system remains completely kinematic in all of its fiber variables.

Since the mechanical connection for the platform plays a role identical to that of the kinematic connection for the robot, we can also plot the height functions for it in the same way that

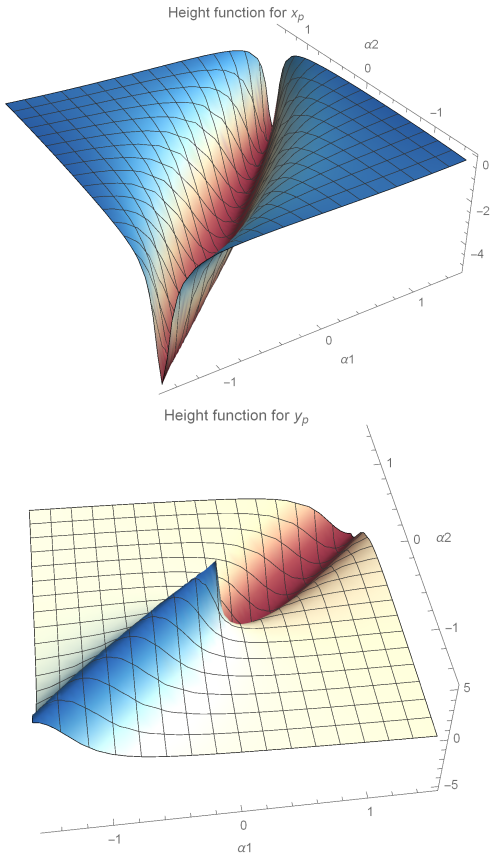

FIGURE 9. THE x AND y HEIGHT FUNCTIONS CORRESPONDING TO THE LOCAL MECHANICAL CONNECTION OF THE PLATFORM. THE MAGNITUDE OF THE x PLOT IS EVERYWHERE OPPOSITE THAT OF THE KINEMATIC CONNECTION OF THE ROBOT; THE SAME IS TRUE FOR THE y PLOT HERE AND THE θ PLOT IN THE FORMER.

we have done for the robot. Fig. 9 shows their shape for a set of chosen system parameters; the top plot is the x_p height function, while the bottom is y_p (unlike the robot, whose second height function is that of θ). The main observation one finds from these plots is that the overall shapes are flipped about zero compared to the robot's height functions. As the robot moves forward in one direction, we would expect the platform to tend to move in the opposite direction. Interestingly, while the platform does not rotate, its y_p height function (motion of the platform in a direction lateral to the robot's heading) looks like the robot's θ function flipped. This is sensible since rotating the robot also rotates the attached body frame, meaning that the initial progression of the platform along the robot's longitudinal direction now rotates into the lateral direction.

An Actuated Platform Now suppose that rather than actuating the robot's joint variables as is usually done, we assume control over the platform fibers (x_p, y_p) (and/or its derivatives). In relinquishing direct control of the robot, the kinematic connection of Eq. (4) is still valid, but the actuation of the platform will affect both the fiber and the base of the robot in a coupled, nontrivial manner. This is in contrast to the case with the passive platform, wherein base trajectories are lifted separately into each of the fiber spaces without any coupling between them.

In the most general case, we will assume that the robot's joints passively follow the dynamics of a mass-spring-damper system. Conversely, we will bypass the dynamics of the platform and assume that we can control its position or velocity directly, setting $m_p = 0$. This leads to a kinetic energy

$$T(q_p, \dot{q}_p) = \frac{1}{2}\sum_{i=1}^{3}\left(m_{l,i}(\dot{\tilde{x}}_i^2 + \dot{\tilde{y}}_i^2) + J_i\dot{\theta}_i^2\right) + \frac{1}{2}\sum_{j=1}^{2} m_{h,j}(\dot{\tilde{x}}_{h,j}^2 + \dot{\tilde{y}}_{h,j}^2)$$

and potential energy

$$U(\alpha) = \frac{1}{2}(k_1\alpha_1^2 + k_2\alpha_2^2),$$

where $(\tilde{x}_{h,j}, \tilde{y}_{h,j})$ is the absolute position of the jth hinge expressed in terms of the configuration variables, and $m_{h,j}$ and k_j are the mass and stiffness coefficient of the jth hinge. The Lagrangian of this system is then written as $\tilde{L}(q_p, \dot{q}_p) = T - U$.

Unlike the previous case of a passive platform, this system is not governed by momentum conservation, as we are injecting energy via actuation into the two fiber components whose momentum were conserved before. We are thus unable to find a reduced set of equations and instead use a set of Euler-Lagrange equations in the form

$$\frac{d}{dt}\left(\frac{\partial \tilde{L}}{\partial \dot{g}_i}\right) = (\omega_g)_i^T \lambda, \tag{7}$$

$$\frac{d}{dt}\left(\frac{\partial \tilde{L}}{\partial \dot{\alpha}_j}\right) - \frac{\partial \tilde{L}}{\partial \alpha_j} = (\omega_\alpha)_j^T \lambda - d_j\dot{\alpha}_j. \tag{8}$$

The object $(\omega_g)_i$ refers to the ith column of ω_g in Eq. (3) (and similarly for ω_r), while the Lagrange multipliers $\lambda \in \mathbb{R}^3$ represent the constraint forces. The constants d_j are damping coefficients and the terms $d_j\dot{\alpha}_j$ are appended to the Euler-Lagrange shape equations to capture the damping model components for each hinge.

Typically we are not concerned with the evolution of the Lagrange multipliers λ. It can be shown that ω_g is full rank away from singular configurations of the robot, so we can use the three equations of (7) to solve for λ and substitute them into (8). The two resultant equations are then

$$\frac{d}{dt}\left(\frac{\partial \tilde{L}}{\partial \dot{\alpha}_j}\right) - \frac{\partial \tilde{L}}{\partial \alpha_j} = \left[(\omega_\alpha)^T(\omega_g)^{-T}\frac{d}{dt}\left(\frac{\partial \tilde{L}}{\partial \dot{g}}\right)\right]_j - d_j\dot{\alpha}_j. \tag{9}$$

Evidently these equations are second-order in all of the configuration variables, and they determine how a trajectory in (x_p, y_p) affects the evolution of the robot's configuration. At the same time, the base and fiber trajectories of the latter must still satisfy the relationship determined by the kinematic connection (4).

Finally, we note that we can write the above equations in an alternative representation that only involves the platform fibers and the base variables. If we choose to specify the platform's velocity using the variables

$$\begin{bmatrix}\dot{u}_p \\ \dot{v}_p\end{bmatrix} = \begin{bmatrix}\cos\theta & \sin\theta \\ -\sin\theta & \cos\theta\end{bmatrix}\begin{bmatrix}\dot{x}_p \\ \dot{y}_p\end{bmatrix}, \tag{10}$$

which is simply a rotation that describes the platform with respect to a frame attached to the moving robot, then we can directly substitute Eq. (4) into (9) and eliminate the explicit dependence on θ. We end up with an equation of the form

$$M(\alpha)\ddot{\alpha} + \dot{\alpha}^T C(\alpha)\dot{\alpha} + N(\alpha) = T(\alpha)\tau, \tag{11}$$

which is a second-order equation in the shape variables α and a set of inputs τ only. M, C, N, and T are matrices of appropriate sizes, and $\tau = (u_p, v_p, \dot{u}_p, \dot{v}_p)^T$ is a vector of inputs. This is analogous to the results in Ostrowski [13], in which a set of second-order shape dynamics complements horizontal lift on the principal bundle. For the present system, this representation is useful if we wish for the platform to be actuated relative to the robot's orientation, rather than in world frame directions. A graphical representation of this system structure is shown in Fig. 10.

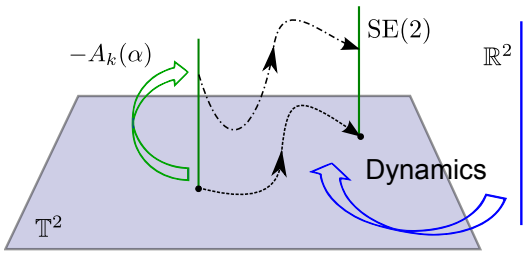

FIGURE 10. THE BUNDLE STRUCTURE OF THE ROBOT AND ACTUATED PLATFORM SYSTEM. ROBOT BASE TRAJECTORIES EVOLVE ACCORDING TO DYNAMICS COUPLED TO THE PLATFORM FIBERS AND LIFT TO THE ROBOT FIBERS.

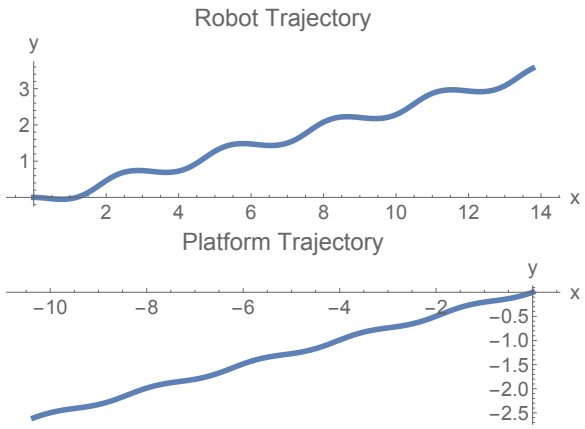

FIGURE 11. ROBOT AND PASSIVE PLATFORM TRAJECTORIES FOR A STANDARD SINUSOIDAL GAIT. AS EXPECTED, THEY GENERALLY MOVE IN OPPOSITE DIRECTIONS.

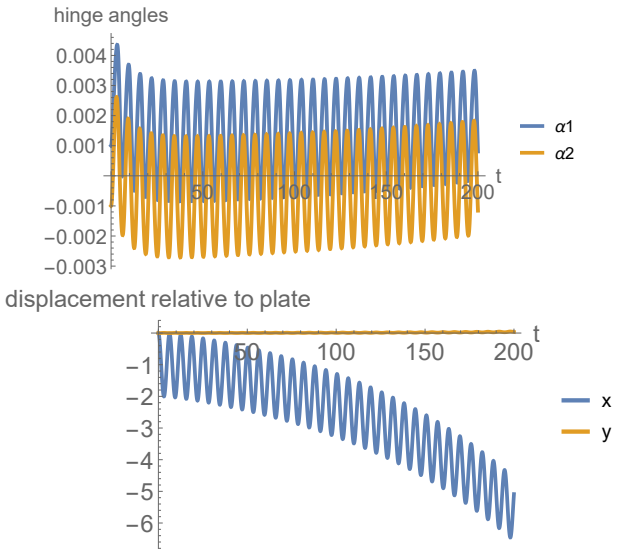

FIGURE 12. ROBOT JOINT AND POSITION TRAJECTORIES FOR PLATFORM VIBRATION AT 45 DEGREES TO THE ROBOT'S INITIAL ORIENTATION. THE JOINT VARIABLES OSCILLATE IN PHASE BUT WITH A NON-CONSTANT OFFSET, ALLOWING FOR NET DISPLACEMENT IN THE ROBOT'S x POSITION. THERE IS NO NET MOTION IN THE y DIRECTION ORTHOGONAL TO THE CONSTRAINTS.

Simulations

For simulations of the previously described robot and platform systems, we set all parameters, including masses, inertias, and damping constants, to 1; in this paper, we leave the spring constants as 0, so as to avoid biasing the robot's resting configuration to be the singular straightened out configuration. While there are possibly richer and more diverse behaviors with different relative parameter values, particularly the damping ratios of the second case, we save that exploration for future work.

Fig. 11 shows the trajectories taken by the robot and passive platform system for the gait $(\alpha_1(t) = \sin t, \alpha_2(t) = \cos t)$. As we had previously propositioned with our height function observations, the two systems tend to move in opposite directions. The wriggling trajectory taken by the robot is a typical locomotion mode for this type of gait. The platform's trajectory is less oscillatory than the robot while maintaining a similar backward-moving component, primarily because the magnitude of the y_p height function is relatively small.

Turning now to the case in which the platform is actuated and the robot is passive, we vibrate the former at an angle of 45 degrees (we set $\ddot{x}_p(t) = \ddot{y}_p(t) = \cos t$) and start the latter near a straight configuration with $\theta = 0$ and $\alpha_1 = -\alpha_2 = \varepsilon$, where ε is small. Fig. 12 shows the resultant trajectories in the robot's base and fiber variables as a result of this choice of induced movement. We can see that the joint angles are generally in phase but are centered around different offsets and never cross each other. Ordinarily, an in-phase trajectory in the base would not yield any net displacement in the fiber for a system governed by a kinematic connection. This can be understood in the height function interpretation from Fig. 7; a completely in-phase gait is linear rather than elliptical and encloses no net area, leading to zero locomotive contribution. However, because the shape trajectories induced by the platform gradually shift over time, each successive gait cycle does not completely wipe out the gains achieved in the previous one. Hence, while we see that the robot is mostly moving back and forth along its body x direction, it is still able to acquire a net displacement away from the origin. Conversely, no net motion occurs in the y direction, since it is mostly orthogonal to the robot's three nonholonomic constraints.

Alternatively, we can control the platform via actuation relative to the robot's configuration by setting $\dot{u}_p$ and $\dot{v}_p$ in Eq. (10). For example, by setting $\ddot{u}_p(t) = \ddot{v}_p(t) = \cos t$, we have the platform vibrate at 45 degrees relative to the robot's body frame. In doing so, we can separately solve for the shape trajectories using the dynamics of Eq. (11), followed by the usual lift to the fiber trajectories via the kinematic connection. This allows us to potentially discover controls for the platform that generate desired joint velocities without worrying about coupling with the fibers.

Example trajectories for this control scheme are shown in Fig. 13. Unlike the previous case, we see that the joint angles end up oscillating out of phase with each other, even though they initially start in-phase as with the previous simulation. This allows the robot to achieve relatively greater displacement in both the x and y directions as compared to before. Again, this may be understood from superimposing the joint trajectories onto the height functions (Fig. 7) of the robot. The out-of-phase joint angles form circular trajectories on the base space that enclose nonzero volume, since both remain positive and in the same

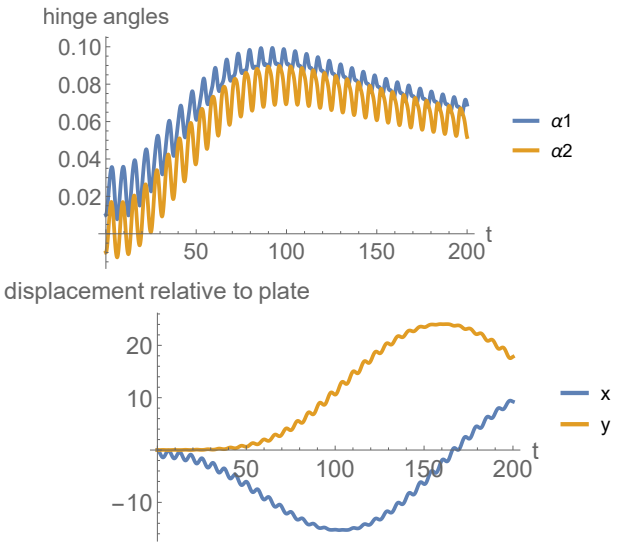

FIGURE 13. ROBOT JOINT AND POSITION TRAJECTORIES FOR PLATFORM VIBRATION AT 45 DEGREES TO THE ROBOT'S CONCURRENT ORIENTATION. THE JOINT VARIABLES OSCILLATE OUT OF PHASE BUT VARY CLOSELY TOGETHER.

quadrant of the space, leading to net rotation of the system. This results in net motion in both the x and y directions.

4 CONCLUSION AND FUTURE WORK

In this paper we have reviewed and expanded upon the principal fiber bundle structure traditionally used to model locomoting systems with a rather limiting set of assumptions and restrictions. In the aquatic locomotion example of a spherical swimmer in a non-symmetric environment, we have shown that the symmetry group may occur in the space of internal shapes rather than on the fibers, allowing for locomotion to occur with only one actuated degree of freedom. The second example is that of the terrestrial snake robot, whose interactions with a movable platform give rise to either a mechanical connection in conjunction with the kinematic connection, or a set of dynamics that couple the system's configuration variables together but simultaneously maintains trajectories compatible with the kinematic connection.

In future work we will continue exploring the space of locomoting systems that do not fit the traditional assumptions of systems on principal bundles. Many robotic systems have symmetric internal degrees of freedom, while others may lack symmetry in some or all of their external degrees of freedom. A number of systems may be controlled via an external source rather than changing internal joints, such as robots in a planar flow or in an electromagnetic field. By extending this framework into the realm of these less than "ideal" systems, we hope to better understand their rich dynamics by carrying over many of the tools already developed in analysis and motion planning for tamer systems.

REFERENCES

[1] Marsden, J. E., and Ratiu, T. S., 1995. "Introduction to mechanics and symmetry". *Physics Today,* ***48***(12), p. 65.

[2] Milne-Thomson, L. M., 1968. *Theoretical hydrodynamics*. Courier Corporation.

[3] Marsden, J. E., Montgomery, R., and Raiu, T. S., 1990. *Reduction, symmetry, and phases in mechanics*, Vol. 436. American Mathematical Soc.

[4] Marsden, J. E., 1992. *Lectures on mechanics*, Vol. 174. Cambridge University Press.

[5] Shapere, A., and Wilczek, F., 1989. "Geometry of self-propulsion at low reynolds number". *Journal of Fluid Mechanics,* ***198***, pp. 557–585.

[6] Shapere, A., and Wilczek, F., 1989. "Efficiencies of self-propulsion at low reynolds number". *Journal of fluid mechanics,* ***198***, pp. 587–599.

[7] Kelly, S. D., and Murray, R. M., 1996. "The geometry and control of dissipative systems". In Decision and Control, 1996., Proceedings of the 35th IEEE Conference on, Vol. 1, IEEE, pp. 981–986.

[8] Kelly, S. D., and Murray, R. M., 1995. "Geometric phases and robotic locomotion". *Journal of Robotic Systems,* ***12***(6), pp. 417–431.

[9] Bloch, A., Krishnaprasad, P., Marsden, J., and Murray, R., 1996. "Nonholonomic mechanical systems with symmetry". *Archive for Rational Mechanics and Analysis,* ***136***(1), pp. 21–99.

[10] Purcell, E. M., 1977. "Life at low reynolds number". *Am. J. Phys,* ***45***(1), pp. 3–11.

[11] Ostrowski, J. P., 1996. "The mechanics and control of undulatory robotic locomotion". PhD thesis, California Institute of Technology.

[12] Ostrowski, J., and Burdick, J., 1996. "Gait kinematics for a serpentine robot". In Robotics and Automation, 1996. Proceedings., 1996 IEEE International Conference on, Vol. 2, pp. 1294–1299 vol.2.

[13] Ostrowski, J., 1999. "Computing reduced equations for robotic systems with constraints and symmetries". *Robotics and Automation, IEEE Transactions on,* ***15***(1), Feb, pp. 111–123.

[14] Shammas, E. A., Choset, H., and Rizzi, A. A., 2007. "Geometric motion planning analysis for two classes of underactuated mechanical systems". *The International Journal of Robotics Research,* ***26***(10), pp. 1043–1073.

[15] Hatton, R. L., and Choset, H., 2011. "Geometric motion planning: The local connection, stokes theorem, and the importance of coordinate choice". *The International Journal of Robotics Research,* ***30***(8), pp. 988–1014.